Chemisorbed Oxygen at Pt(111): a DFT Study of Structural and Electronic Surface Properties

Ali Malek[1] . Michael H. Eikerling[1]

Department of Chemistry, Simon Fraser University, Burnaby, BC V5A 1S6, Canada

* Corresponding author. Phone: +1-778-782-4463, email: meikerl@sfu.ca

Final version published as:
Malek, A. & Eikerling, M.H. Chemisorbed Oxygen at Pt(111): a DFT Study of Structural and Electronic Surface Properties. *Electrocatalysis* (2018) 9: 370-379.
https://doi.org/10.1007/s12678-017-0436-0

ABSTRACT

Simulations based on density functional theory are used to study the electronic and electrostatic properties of a Pt (111) surface covered by a layer of chemisorbed atomic oxygen. The impact of the oxygen surface coverage and orientationally ordered interfacial water layers is explored. The oxygen adsorption energy decreases as a function of oxygen coverage due to lateral adsorbate repulsion. The surficial dipole moment density induced by the layer of chemisorbed oxygen causes a positive shift of the work function. In simulations with interfacial water layers, ordering and orientation of water molecules strongly affect the work function. It is found that the surficial dipole moment density and charge density are roughly linearly dependent on the oxygen surface coverage. Moreover, we found that water layers exert only a small impact on the surface charging behavior of the surface.

INTRODUCTION

Platinum (Pt) is a critical materials component in polymer electrolyte fuel cells (PEFCs) and other emerging electrochemical energy technologies.[1-4] Notwithstanding decades of intense research on replacement materials[3, 5, 6], Pt remains the best-performing metal-based catalyst for the oxygen reduction and the oxygen evolution reactions (ORR and OER), when they are performed in aqueous acidic environment.[7-9]

From a techno-economic perspective, Pt is however far from ideal as an electrocatalyst. Even with the use of significant amounts of Pt, the ORR at the cathode catalyst layer incurs voltage losses of 0.3 to 0.4 V under normal PEFC operation.[2] Moreover, Pt accounts for 20 to 40% of the cost of a fuel cell stack.[10, 11] In spite of the critical impact on cost and performance, it turns out that Pt is heavily underutilized in the cathode catalyst layer of a PEFC, as indicated by the low value of the effectiveness factor of Pt utilization; independent experimental[12] and modeling studies[13] pinpoint the value of this vital metric in the range of 5% or even below. The related issues of high materials cost and poor effectiveness factor are aggravated by another challenge, namely the degradation of the catalytic performance caused by dissolution, coagulation and detachment of Pt nanoparticles.[14-17]

Forays in electrocatalysis research therefore strive to rationalize the factors that control the ORR activity of Pt-based catalysts[18-20] and they increasingly place a focus on

unraveling the critical correlation between ORR activity and Pt dissolution kinetics.[21-23] In this context, the mechanisms and rates of the ORR and Pt dissolution are intimately linked as they both proceed through the formation or reduction of chemisorbed oxygen species at the Pt surface.[24-27] Knowing the precise surface adsorption and oxidation state of Pt as a function of electrode potential is thus a vital prerequisite in any attempt to unravel the catalytic function of Pt.[28, 29] In this realm, we must scrutinize how adsorption and oxidation processes affect electronic, electrostatic and electrocatalytic properties of the Pt surface.[3]

Finding the self-consistent solution for the fundamental correlations in Pt electrocatalysis, outlined in the previous paragraph, is the central subject of theoretical research and first principles simulations.[3] The Pt electrode potential, ϕ^{Pt}, is the primary variable that controls the surface adsorption and oxidation state and associated electrostatic charging properties of the metal-solution interface, including the surface charge density, surface dipole moment density and higher moments of the charge density distribution. These charging properties in turn determine the spatial distributions of electrostatic potential and proton density in the adjacent electrolyte phase. A theoretical framework to self-consistently calculate the potential distribution across the metal-solution interface was recently proposed by Huang *et al.[30]*.

Over the last decade, several first principles electrochemical simulations based on density functional theory (DFT) have started to address this challenge.[31-34] It is

straightforward in such studies to specify an electrode surface structure and an adsorbent coverage or to control the surface charge density.[35-37] The principal difficulty in all of these approaches is that ϕ^{Pt} hitherto cannot be controlled in quantum chemical calculations. Another challenge for self-consistent simulations of the metal-solution interface is the treatment of solvent effects. Solvent effects can be treated explicitly, using first principles simulations that account for molecular structure, distribution, and orientation of solvent molecules and their specific interactions with the metal surface, as done for instance in Ref.[38]. Alternatively, solvent effects can be incorporated implicitly by describing the solvent as a continuous medium with effective properties.[38, 39] In a recent study by Gray *et al*. [39] adsorption energies of H, O and OH adsorbates at a Pt(111) surface were calculated and compared under gas-phase and solvated conditions for periodic slab and surface cluster models. For the adsorption of atomic H and O at the Pt(111) surface, the solvent effect was found to incur small corrections to the calculated adsorption energies. These corrections were around 0.07 and 0.17 eV for adsorption of H and O at fcc-hollow surface sites, respectively.

The solvent affects the electrode charging behavior as well as ion density and potential distributions in the interfacial electrolyte region by virtue of its dielectric properties. Moreover, the orientational ordering of interfacial water molecules exerts a significant impact on the electronic structure and charging behaviour of the interface, as seen in DFT studies with explicitly considered water layers [40-44] and rationalized in the theory

developed by Huang *et al*.[30]

Both experimental and theoretical findings suggest that surficial water on transition metals organizes spontaneously into an ordered structure with hexagonal ice-like configuration.[45-50] On Pt(111), a water monolayer forming a 2D H-bonded network was confirmed to be stable at low temperature by UHV experiments and theoretical calculations.[51]

The aim of the present study is to explore the impact of oxygen chemisorption at Pt as well as the presence of explicit water layers on the electronic and electrostatic charging properties of the catalyst surface, focusing on the low-temperature water configuration. We present a DFT study of Pt(111)-O_{ad} and Pt(111)-O_{ad}-H_2O structures for varying coverage by chemisorbed oxygen. Moreover, we evaluate the impact of ice-like surface layers of water molecules that differ in the orientation of the water dipole towards the Pt-O_{ad} surface. DFT results for these systems will be analyzed in view of adsorption energy, work function shift, and electrostatic properties.

COMPUTIONAL DETAILS

Periodic DFT calculations were performed with the Vienna Ab initio Simulation Package, VASP,[52-55] utilizing the generalized gradient approximation (GGA) with the revised Perdew-Burke-Ernzerhof (revPBE) exchange correlation functional[56, 57] and treating valence electrons with the projector augmented wave (PAW) method.[58] The cut-off

energy of the plane-wave expansion was 400 eV. Total-energy calculations were done with the block Davidson iteration method for electronic relaxation. Geometry optimizations were considered as converged when the force on each atom was less than 0.02 eV/ Å.

Calculations were performed for Pt(111) slabs with (2×2), (3×3), (4×4) or (2√3× 2√3) R30° surface unit cells. The difference in the adsorption energies between three and four layers and four and five layer slabs were as high as 0.03eV per O atom, while the difference in adsorption energies between five and six layers was less than 0.01 eV per O atom. Therefore, calculations were performed using five layer slabs. [59, 60]

The different unit cells considered allowed O_{ad} coverages in different intervals in the range of 0.062-1.0 ML to be studied. Fig. 1 shows the (4x4) Pt(111) surface with different adsorbate amounts and configurations. Brillouin zone integrations were performed for Monkhorst–Pack grids of 2×2×1, 4×4×1, 6×6×1, 9×9×1, 11×11×1, with a Fermi-level smearing of 0.2 eV using the Methfessel–Paxton scheme. The bottom two layers of the Pt slab were fixed in their bulk positions, while the upper part of the slab was allowed to relax in response to O_{ad} formation.

The calculations were performed with the equilibrium lattice constant a_0 = 4.02 Å. A dipole correction was imposed to eliminate the error induced by the artificial electrostatic interaction between the surface dipole moments of asymmetric repeated slabs.[61] A

vacuum region of about 16 Å ensures that a slab does not interact with its periodic image in the surface-normal direction.

Adding an explicit ice-like monolayer or two monolayers of water further modified the interfacial system, evaluated for the (3×3) unit cell. Water molecules in the monolayer adjacent to the surface were considered to organize in H-up and H-down water structures. In the H-up structure, the O-H bonds of water molecules in the first layer point away from the surface, and in H-down structure the dangling O-H bonds in the first water layer are directed at the surface. The first water monolayer was fully relaxed, whereas molecules in the second water monolayer were frozen in x and y direction.

Unit cell: 4x4

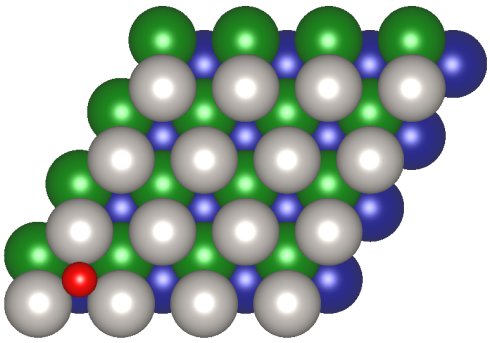

$\theta = 0.0625$ ML

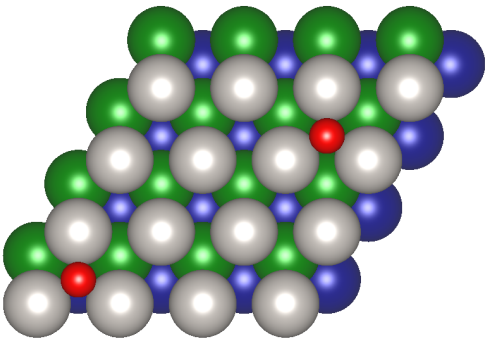

$\theta = 0.12$ ML

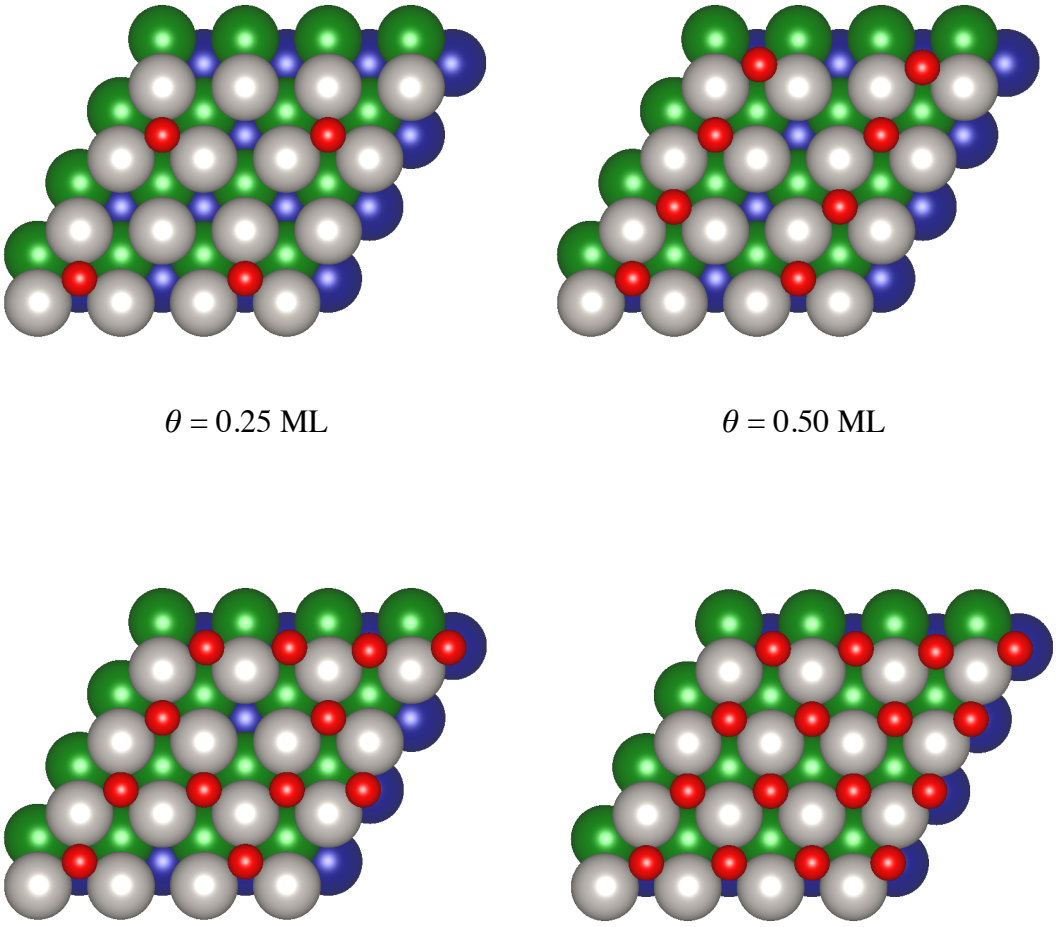

Fig. 1 Atomic structure of oxygen adsorbed on Pt(111) at varying surface coverage, θ, for the (4x4) unit cell. The oxygen atoms are depicted in red and Pt atoms in first, second and third layers of the Pt slab are shown with grey, green and dark blue color, respectively.

RESULTS AND DISCUSSION

On Surface Adsorption

The energetically favored oxygen-adsorption sites on Pt (111) are the fcc sites.[62] For oxygen adsorption on the surface, we explored the fcc-hollow sites in the coverage range from 0.06 to 1.00 ML for the (2×2), (3×3), (4×4), or (2 √3× 2 √3) R30° surface unit cells. The surface coverage of oxygen is defined as $\theta = \frac{N_O}{N_{Pt}}$, where N_O represents the number of adsorbed oxygen atoms and N_{Pt} the number of Pt surface atoms in the unit cell. The oxygen adsorption energy, $\Delta E_{avg}(\theta)$, was calculated from the following expression,

$$\Delta E_{avg}(\theta) = \frac{1}{N_O}\left[E_{O/Pt(111)} - E_{Pt(111)} - \frac{N_O}{2} E_{O_2} \right]. \quad (1)$$

Here, $E_{O/Pt(111)}$, $E_{Pt(111)}$, and E_{O_2} are total energies of Pt(111)-O_{ad},clean Pt(111) surface, and an O_2 molecule in the gas phase, which were calculated from DFT simulations. Fig. 2 shows $\Delta E_{avg}(\theta)$ as a function of θ. As can be seen, the absolute value of $\Delta E_{avg}(\theta)$ decreases with θ. This trend is caused by the electrostatic repulsive interaction between neighboring O adatoms and the increasing competition for d-orbital electrons of Pt surface atoms that participate in the Pt-O_{ad} bonding. The Frumkin interaction factor, $f = r / RT$, is obtained using $r(\theta, T) = \left(\frac{\partial \Delta E_{avg}}{\partial \theta} \right)_T$. Linear regression of the data in Fig. 2 gives r = 1.2 eV for 0.1 < θ < 1.0 and thus f = 45.2 at T = 298.2 K. This value agrees well with the value 41.5 obtained from the experimental analysis performed in Ref.[63]

in the range $0.0 < \theta < 0.3$. Fig. 2 shows that the size of the unit cell has a weak influence on $\Delta E_{\mathrm{avg}}(\theta)$. The most significant difference is found for the (2√3× 2√3) R30° surface, which exhibits a different surface configuration of adsorbed O atoms.

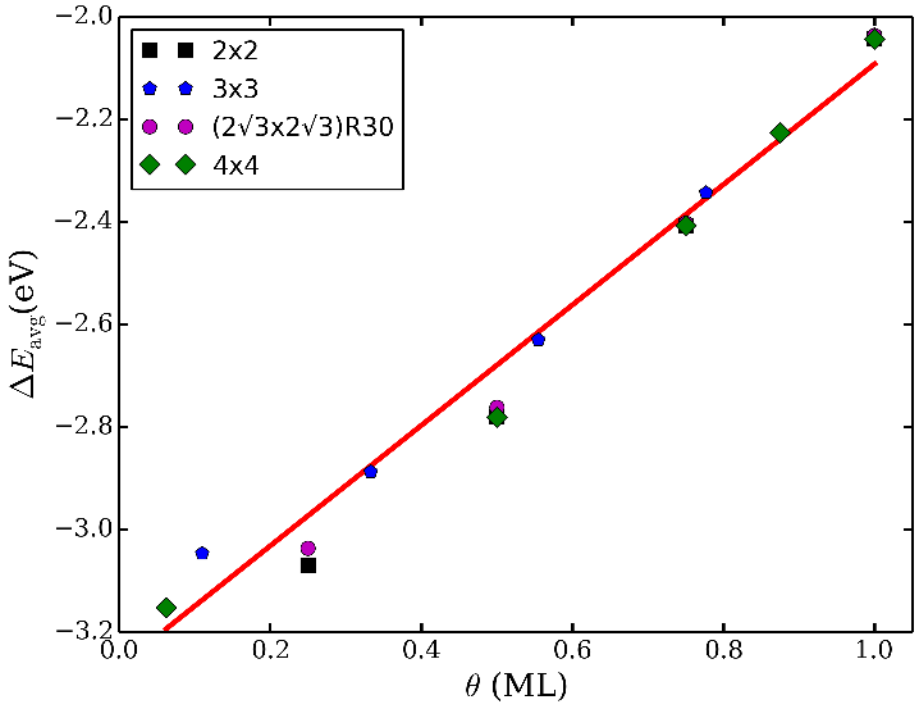

Fig. 2 Calculated average adsorption energy of atomic oxygen on Pt(111) at fcc-hollow sites, plotted over the oxygen surface coverage for the different unit cell sizes considered in this work. The solid line shows the interpolation of adsorption energies obtained for all unit cells.

Electronic and Electrostatic Properties

Work Function Change and Surface Dipole Moment

To investigate the electronic properties of the Pt(111)-O_{ad} system, in the first step we evaluated the change in the work function as a function of θ, as shown Fig. 3. The work function can be formally decomposed as

$$\Phi = e_0\chi - E_F, \tag{2}$$

with e_0 being the elementary charge, E_F the Fermi energy of the metal and χ the surface potential due to the formation of a Helmholtz-like $Pt^{\varsigma+} - O^{\varsigma-}$ dipole layer, where ς is the fractional charge number. The work function at each value of θ is calculated as the difference of the electrostatic energy of an electron in the center of the vacuum slab above the oxidized surface to the Fermi energy, E_F, of the clean Pt(111) slab. The work function change upon formation of O_{ad}, relative to the value obtained for the clean surface of Pt(111), is

$$\Delta\Phi = \Phi_{O/Pt(111)} - \Phi_{Pt(111)} = e_0\Delta\chi, \tag{3}$$

where $\Phi_{O/Pt(111)}$ is the work function of the Pt(111)-O_{ad} system and $\Phi_{Pt(111)}$ is the work function of the clean Pt surface. Calculated work function values of the pristine Pt(111) surface are 5.67, 5.68, 5.64, and 5.60 eV for 2x2, 3x3, ($2\sqrt{3}\times 2\sqrt{3}$) R30° and 4x4 unit cells, respectively. These values agree well with various experimental reports that obtained work function values in the range from 5.6 eV to 6.1 eV. [44, 64-67]

It can be seen in Fig. 3 that the work function increases nearly linearly with θ. Values of $\Delta\Phi$ calculated with DFT for the different unit cells are compared with the experimental

values reported in ref. [68]. The agreement is very good

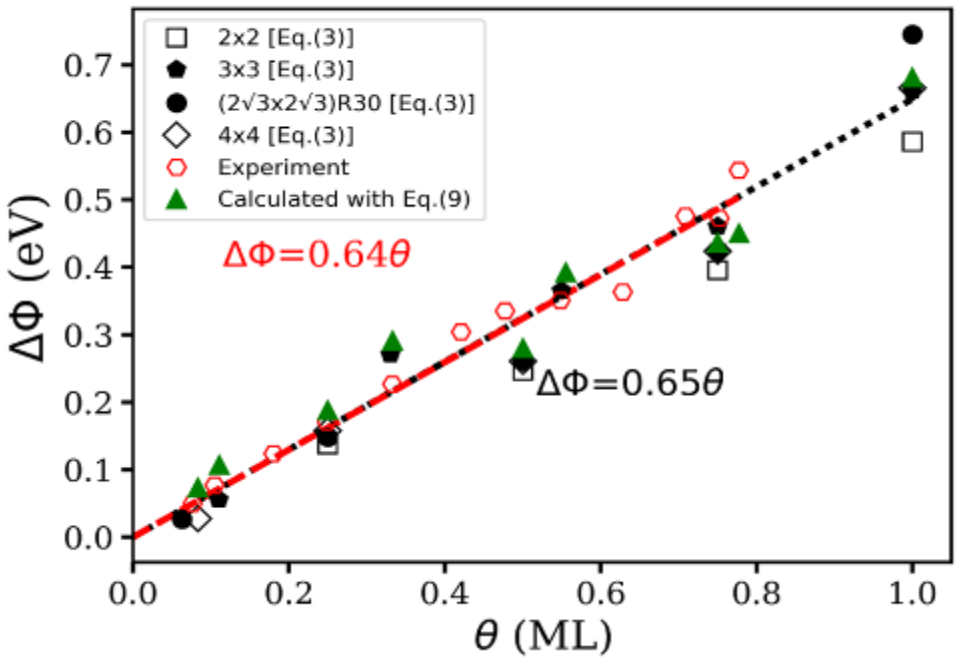

Fig. 2 Change in work function, $\Delta\Phi$, as a function of oxygen surface coverage at fcc-hollow sites of Pt(111)-O for the different unit cell sizes in comparison with experimental data extracted from ref. 68. The triangle-up symbol show the values of the work function change obtained using the Helmholtz-equation, Eq.(9) with the dipole densities taken from Fig. 5. The red dashed line and black dotted line represent a linear regressions of experimental and calculated work function change respectively.

Periodic boundary conditions lead to artificial interactions between dipoles of repeated slabs. The dipole correction scheme of Neugebauer and Scheffler was applied to eliminate the effect of these interactions.[69] To evaluate the accuracy of this approach, we have calculated the work function change also for symmetric slabs, i.e., with oxygen

adatoms chemisorbed on both sides. A dipole correction is not needed in this case. Calculations for symmetric slabs without dipole correction systematically overestimate the work function change, relative to the values obtained for symmetric slabs as well as to experimental data, as documented in Table 1.

A possible reason for the larger discrepancy to experiment as seen for the symmetric slabs could be the larger drift of the Fermi-level of electrons in the centre of the slab owed to the need to freeze two layers of Pt in these systems as opposed to one frozen Pt layer in the centre of asymmetric slabs. It should be possible to eliminate this discrepancy by increasing the number of Pt layers in the slab sufficiently so that work function changes could be extrapolated to the limit of infinite slab thickness. Further improvement in the accuracy of calculated work function changes should be achievable by inclusion of long-range forces or quantum-size effects related to the slab thickness.[70-73] In experiment, the main source of inaccuracies in measuring the work function is the presence of surface defects or adsorbed impurities.[72, 74] Moreover, in experiment, the work function depends on environmental conditions, such as pressure and temperature.[75, 76]

The sign and magnitude of $\Delta\Phi$ can be related to the surficial dipole density. The dipole moment of the $Pt^{\varsigma+} - O^{\varsigma-}$ layer is directed towards the metal surface, corresponding to an increase in $\Delta\Phi$.

Electrostatic properties of the Pt(111)-O_{ad} layer

The electron density redistribution upon formation of adsorbed O can be analysed based on the following expression,

$$\Delta\rho(x,y,z) = \rho_{\mathrm{PtO}}(x,y,z) - \rho_{\mathrm{Pt'}}(x,y,z) - \rho_{\mathrm{O'}}(x,y,z) \tag{4}$$

where $\rho_{\mathrm{PtO}}(\mathbf{r})$ is the electron density in the interacting metal-adsorbate system and $\rho_{\mathrm{Pt'}}(\mathbf{r})$ and $\rho_{\mathrm{O'}}(\mathbf{r})$ are electron densities of the bare Pt surface and of the bare oxygen atoms that form the oxide layer, respectively. The prime indicates that electron density calculation, the geometry of Pt and O atoms are held fixed at positions of the Pt(111)-O_{ad} system.

Fig. 4 shows the plane-averaged electron density difference in z-direction, $\Delta\lambda(z)$, calculated from

$$\Delta\lambda(z) = \int_{-a/2}^{a/2} \mathrm{d}x \int_{-b/2}^{b/2} \Delta\rho(x,y,z)\mathrm{d}y\,, \tag{5}$$

for the (2×2) unit cell. Fig. 4 reveals a discernible, albeit smaller than expected, amount of electron depletion at the top layer of Pt and a corresponding electron accumulation centered slightly above the plane of oxygen adatoms.

As can be seen in Fig. 4, the profile of the charge redistribution at different θ is similar. By increasing θ, the accumulation of electron density around the plane of O adatoms

increases. While overall, oxygen atoms gain electron density from Pt, there is a depletion of electron density in the outer "tail" region of the oxygen layer. The amount of positive charge inside this tail region is however negligible.

The amount of the fractional charge, $Q_{\mathrm{uc}}^{\pm}$, involved in the formation of the interface dipole along the surface normal can be calculated as

$$\begin{cases} Q_{\mathrm{uc}}^{+} = -e_0 \int_{Z_{\mathrm{M}}}^{Z_0} \Delta\lambda(z)\mathrm{d}z, \\ Q_{\mathrm{uc}}^{-} = -e_0 \int_{Z_0}^{Z_{\mathrm{V}}} \Delta\lambda(z)\mathrm{d}z, \end{cases} \tag{6}$$

where Z_{M} is the center of the slab, Z_{v} the middle of the vacuum region between periodically repeated slabs and Z_{0} the position of the z-plane that separates positive and negative excess charge densities. This plane is defined as a position in the region between the top layer of Pt atoms and the oxide layer where $\Delta\lambda(z)$ is zero.

Q_{UC}^{+} is the amount of partial positive charge due to electron depletion on Pt atoms and Q_{uc}^{-} is the amount of partial negative charge due to excess electron accumulation in the O adlayer. The thickness of the dipole layer, δ_{PtO}, is the distance between the centers of positive and negative excess charges, as indicated in Fig. 4.

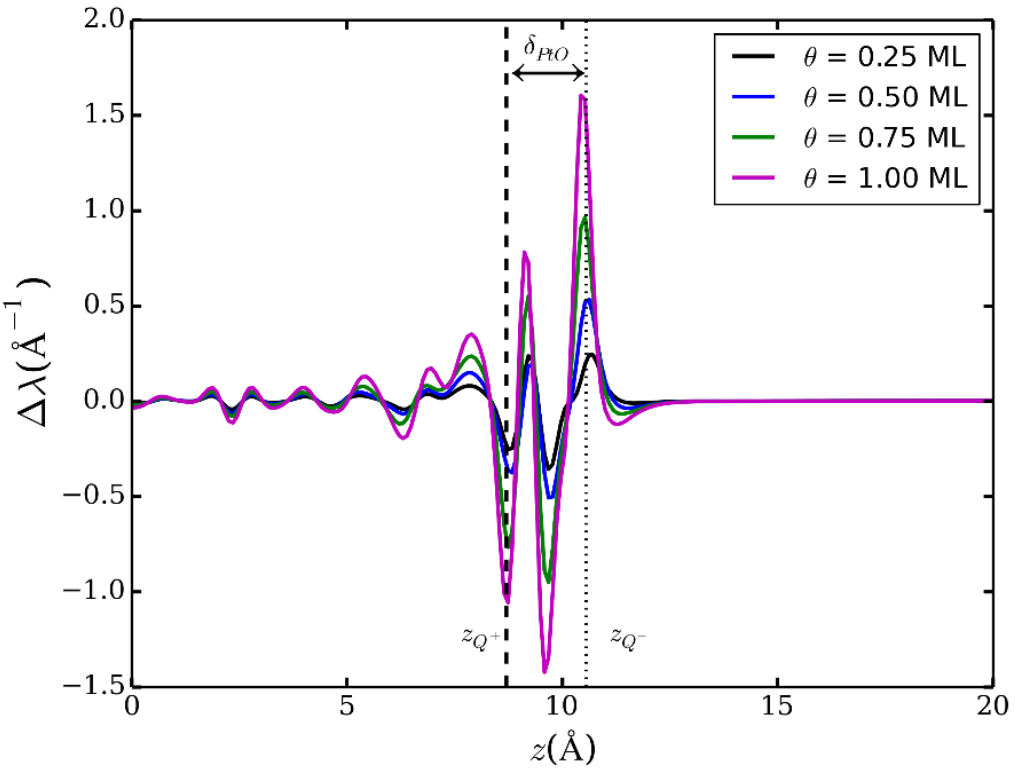

Fig. 3 Variation of the plane-averaged line charge density redistribution along z, calculated according to Eq. (4) for the (2x2) unit cell; z_{ϱ^+} and z_{ϱ^-} indicate the centroids of the positive and negative charge densities, respectively; their positions define the thickness of the dipole layer, as indicated.

The calculated value $\delta_{\mathrm{PtO}} \cong 1.8$ Å is a good approximation at all coverages considered. The surficial oxide dipole moment density, $\mu_{\mathrm{PtO}}[\mathrm{D/Å}^2]$, induced by the chemisorbed layer of O adatoms can be defined as

$$\mu_{\mathrm{PtO}} = N_{\mathrm{tot}}\mu_{\mathrm{site}}, \tag{7}$$

with N_{tot} as the planar atom density of Pt(111), which is given by $4/\left(\sqrt{3}a_{\mathrm{Pt}}{}^2\right)$, where

a_{Pt} = 4.02 Å is the lattice constant. In Eq.(7), the surface averaged dipole moment per Pt oxide couple is

$$\mu_{\mathrm{site}} = -\frac{\theta e_0}{n_{\mathrm{O}}} \int_{Z_M}^{Z_V} z \Delta\lambda(z) \mathrm{d}z \,. \qquad (8)$$

The arithmetic mean of parameters obtained from different unit cells is listed in Table 2. The average value of ς, assigned to a single Pt-O oxide pair which can be found as $\varsigma = \frac{Q^{+}_{\mathrm{uc}}}{n_{\mathrm{O}}} = \frac{Q^{-}_{\mathrm{uc}}}{n_{\mathrm{O}}} = 0.012 e_0$. This value is in good agreement with the average charge (ς=0.01 e_0) that reported by Hyman and Medlin [77] in a DFT study on the adsorption of atomic oxygen at a Pt(111) surface. Moreover, they found that the dipole moment for θ = 0.25 was 0.04 eÅ per Pt-O pair while $\delta_{\mathrm{PtO}} \cong 2$ Å.

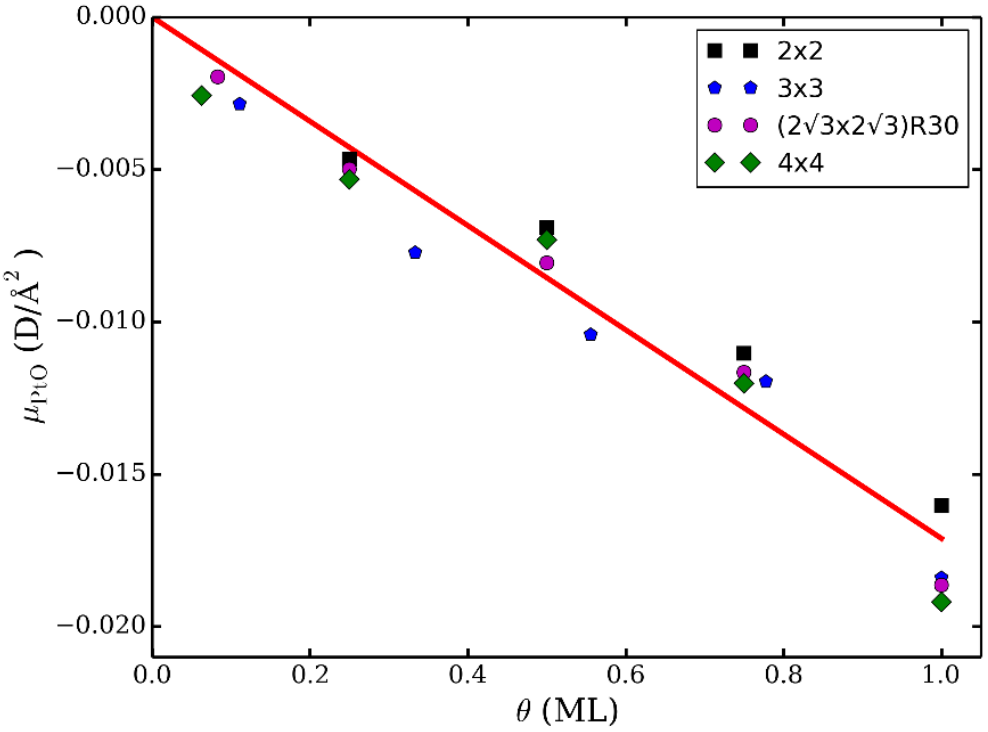

Fig. 4 Calculated average surficial dipole moment per surface area, μ_{PtO}, as a function of oxygen surface coverage for different unit cell sizes. The red line represents a linear regression of the displayed data points.

The surficial dipole density μ_{PtO}, obtained from Eq. (7) and shown in Fig. 5, varies from 0.002 D/Å^2 to 0.019 D/Å^2 for the range of θ values displayed. The surficial dipole density, obtained from a cubic spline interpolation of data points for all unit cell sizes is shown in Fig. 5 as a function of θ. The results in Fig. 5 are in good agreement with the experimental value reported in Ref[68].

The work function change is related to the surficial oxide dipole density via the so-called Helmholtz-equation[67, 78]

$$\Delta\Phi = \frac{e_0 \mu_{PtO}}{\varepsilon_0 \varepsilon}, \qquad (9)$$

where ε_0 and ε are the dielectric permittivity of vacuum and the relative dielectric constant. Since polarization effects due to variations in the surface electronic structure are calculated from first principles, we should use a value of ε = 1 in Eq. (9). With this value, we obtain $\Delta\Phi \approx 0.20$, 0.27, 0.45 and 0.72 eV for θ = 0.25, 0.50, 0.75 and 1.0 ML for the (4x4) unit cell. The values of $\Delta\Phi$ calculated from Eq. (9) with the surficial dipole moment density from Fig. 5 are compared with the values of $\Delta\Phi$ obtained from Eq.(3) in Fig. 3. The results agree very well with the values of $\Delta\Phi$ determined from experiment.

Water Adsorption on the Pt(111)-O_{ad} surface

This section explores the impact of adding two layers of water molecules at the Pt(111)-O_{ad} surface will be explored. Fig. 6 displays H-up and H-down configurations of hexagonal ice-like water molecules on (3x3) Pt(111) unit cell size.

Our DFT calculations show that water monolayers in both H-down and H-up configurations, with a coverage of 2/3, do not form a chemical bond with the Pt (111)-O

surface. The water monolayers are located at a distance of about 4.5-5 Å above the Pt(111)-O_{ad} surface.

(a) (b)

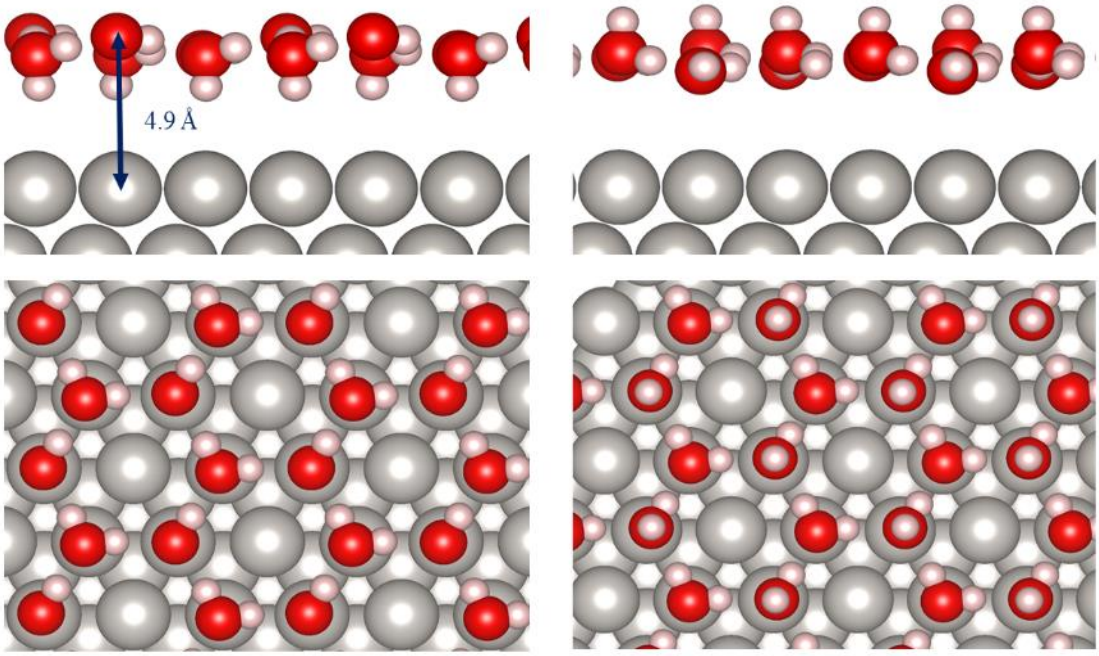

Fig. 5 Ice-like structure of a single monolayer of water on the Pt (111) surface in top and side views for (a) H-up and (b) H-down orientation.

It is known that the work function of Pt is modified upon immersion into a solvent.[44, 79] The calculated work function change for the H-up and H-down configurations on Pt(111) are -2.34 and -0.22 eV, respectively. The experimental value for the work function change due to water adsorption obtained by IR-reflection spectroscopy under grazing incident and by UV-photoemission is 1.2 eV, which lies between the values

obtained for the perfectly oriented water layers in H-up and H-down configuration.[80, 81] This observation can be ascribed to the thermally induced disorder in water orientation that is reflected in the experimental value. [41, 82]

Fig. 7 displays $\Delta\Phi$ for the range of θ values considered in this work, calculated using Eq. (3). Dipole moments of the oppositely oriented water layers in H-up and H-down configuration lead to different shifts of the work function [41].

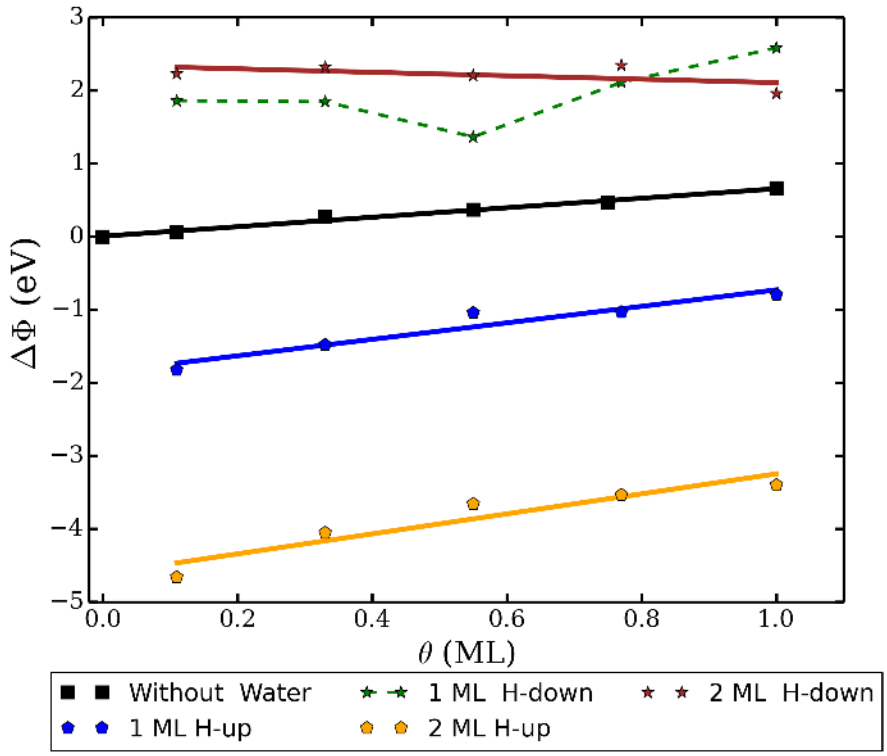

Fig. 6 Calculated work function change as a function of oxygen surface coverage for systems with one and two monolayers of water at the Pt(111)-O surface for different configurations of ice-like water for the (3x3) unit cell of Pt(111).

Work function change upon addition of 1 ML of water in H-up configuration is from - 1.8 eV to -0.8 eV relative to the work function change of bare Pt(111)-O_{ad} . In the case of 1 ML of water in H-down configuration, an enhancement of the work function change by 1.9 to2.6 eV is observed. When two water monolayers are adsorbed, $\Delta\Phi$ for the H-up case will be significantly reduced while $\Delta\Phi$ for the H-down case exhibits a slight increase. Note that there is a large discrepancy between the calculated $\Delta\Phi$ for H-down and H-up configurations with experimental values.[80] This discrepancy could be significantly reduced if thermal motion of water molecules were considered.[41, 82]

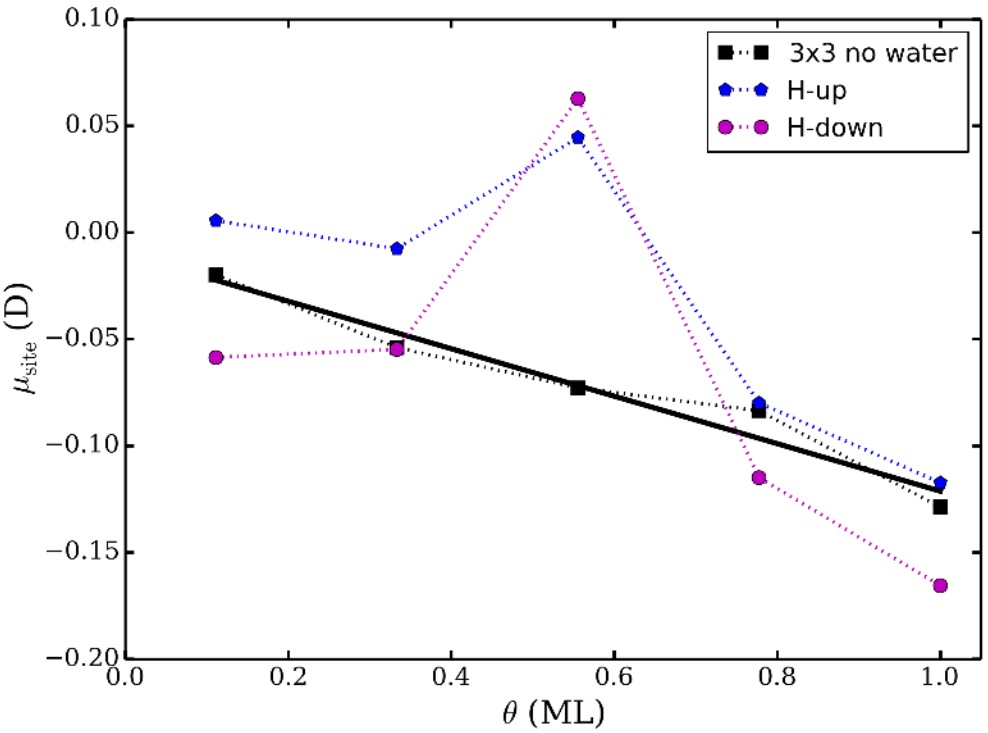

Fig. 7 The calculated average dipole moment as a function of oxygen surface coverage in the

presence of one monolayer of water in H-up and H-down orientation for the (3x3) unit cell of Pt(111).

Fig. 8 displays the average surficial dipole moment per Pt surface atom site, μ_{site}, for simulations with 1 or 2 ML of water in H-up or H-down configuration for the (3x3) unit cell. Results do not exhibit a significant impact of the water layers. Likewise, the charge density redistributions are essentially unaltered in the presence of water monolayers as shown in Fig. 9 (b). This observation suggests that there is a less significant interaction of the water layer with Pt oxide due to the significant distance of water molecules from the Pt surface. Moreover, in order to capture interaction effects of additional water layers, it will be necessary to account for semi-empirical dispersion corrections in simulations.[83]

Fig. 10 show the surface charge density (free charge per area),

$$\sigma = \frac{q}{A_{\text{uc}}}, \tag{10}$$

where q denotes the total net surface charge in the unit cell. The charge density is negative at all θ and it decreases with θ. This trend is consistent with the theoretically obtained result in Ref..[30]

As shown in Fig. 10 there is no difference in the calculated surface charge density between Pt(111)-O_{ad} and Pt(111)-O_{ad}-H_2O. The surface charge densities obtained with 1 ML of water in H-down or H-up configuration are almost identical. As shown in Fig. 10,

(a)

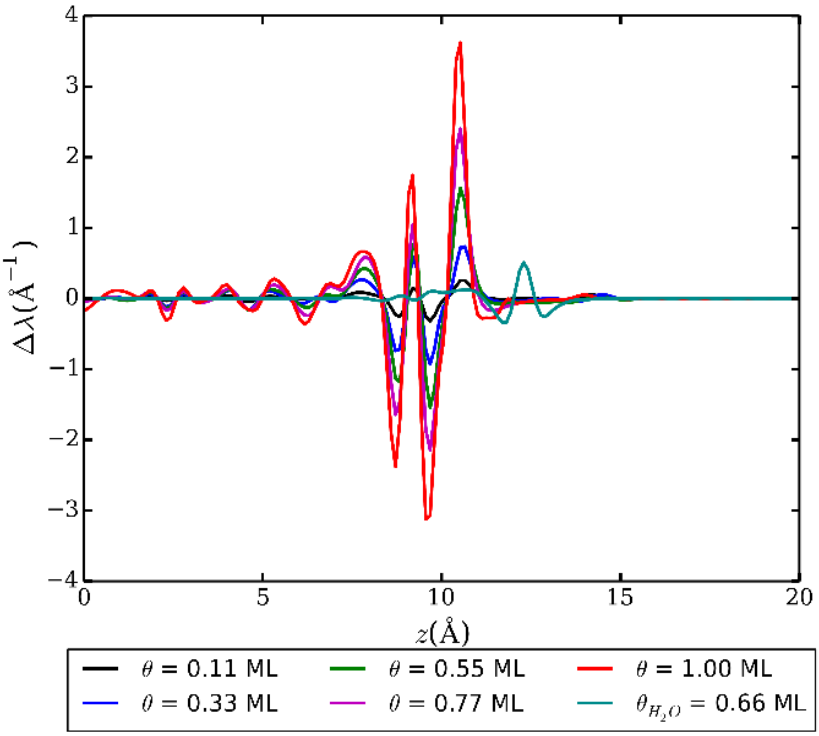
$\Delta\lambda(\text{Å}^{-1})$
z(Å)
θ = 0.11 ML
θ = 0.55 ML
θ = 1.00 ML
θ = 0.33 ML
θ = 0.77 ML
θ_{H_2O} = 0.66 ML

(b)

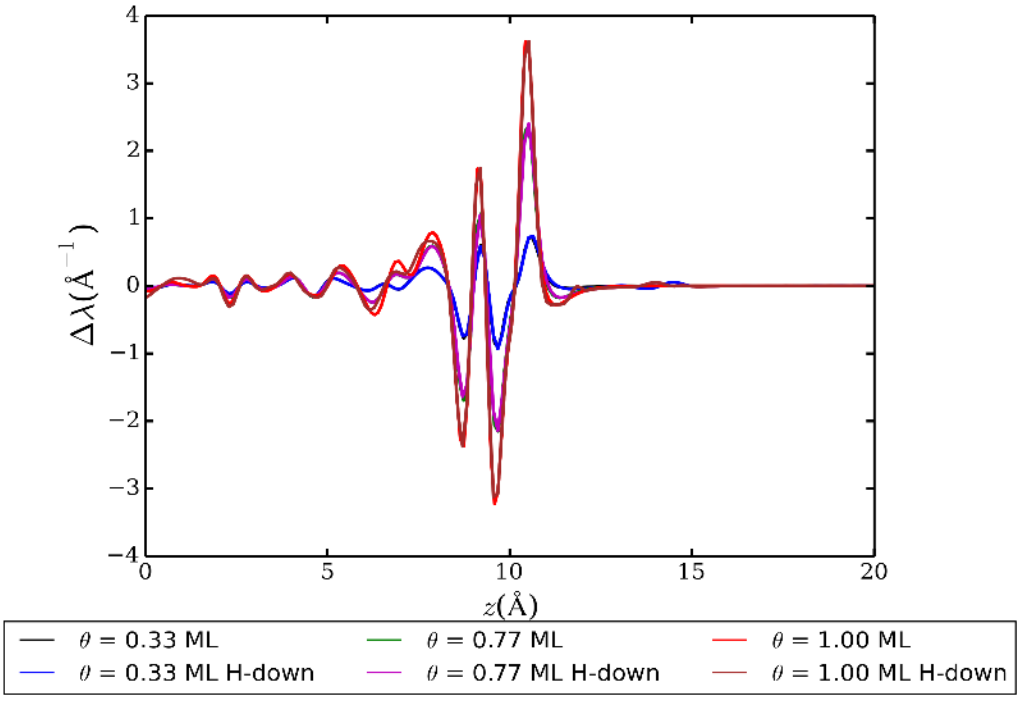
$\Delta\lambda(\text{Å}^{-1})$
z(Å)
θ = 0.33 ML
θ = 0.77 ML
θ = 1.00 ML
θ = 0.33 ML H-down
θ = 0.77 ML H-down
θ = 1.00 ML H-down

Fig. 9 (a) Plane-averaged line charge density redistribution calculated according to Eq. (5) for the Pt(111)-O system with (a) one monolayer of water in H-down orientation. (b) Plane-averaged line charge density redistribution between surface system with and without one monolayer of water in H-down orientation for the (3x3) unit cell of Pt(111)

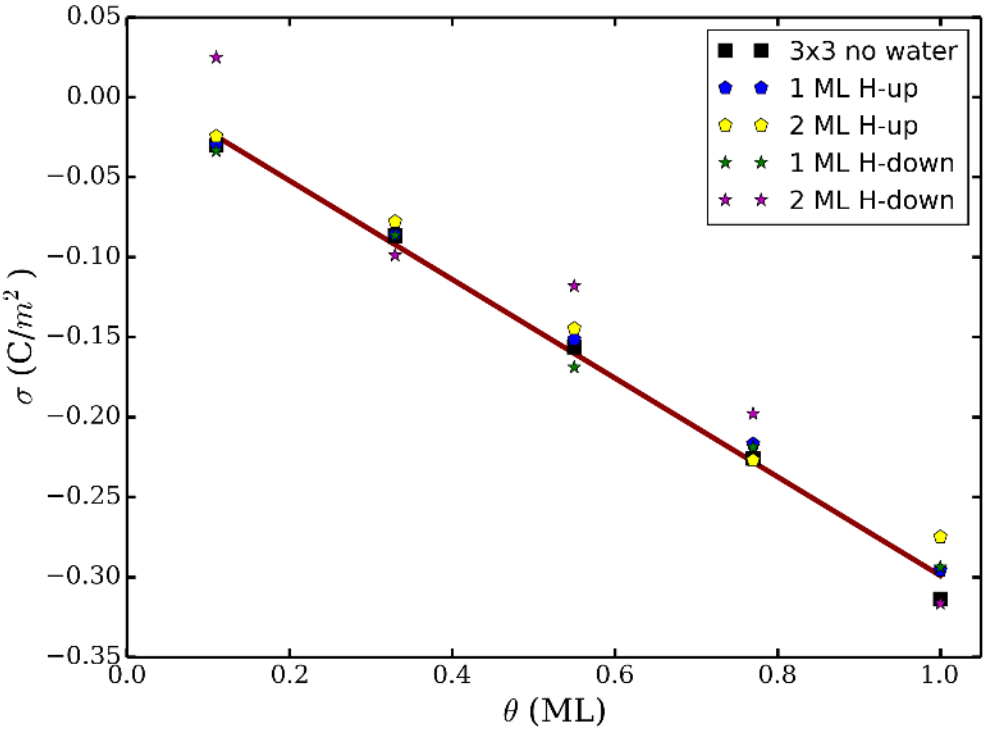

Fig. 10 Calculated surface charge density as a function of oxygen surface coverage for different configurations of one or two monolayers of ice-like water for the (3x3) unit cell. The dark red line represents a linear regression of the displayed points.

there is a small effect upon addition of 2 ML of water in H-up configuration. In general,

we found only a minor impact of added water layers on the surface charging behavior.

CONCLUSIONS

We have presented a detailed theoretical study of the energetic and electrostatic properties of a Pt(111) surface modified by chemisorbed O adatoms and one or two explicitly treated water layers. Analysis of the average adsorption energy of oxygen allows a Frumkin interaction factor to be extracted that agrees with experimental values. The change of the work function correlates roughly linearly with the O adatom surface coverage. Assuming perfectly oriented water layers in H-up or H-down configuration overestimates the impact of the water layers on the work function. It will be necessary to account for thermally induced disorder in water orientation. The analysis of charge density distributions at the surface revealed the linear relations between surficial dipole density and charge density at the surface. The surface charge density is negative and it decreases with oxygen surface coverage.

The properties studied are essential in order to adequately define local reaction conditions that prevail at the metal surface and they thus have vital implications for the mechanisms and kinetics of electrocatalytic surface reactions. The results of these DFT studies are needed as essential input for a recently developed structural model of the Pt|solution interface that self-consistently treats polarization effects caused by surface-adsorbed oxygen species and interfacial water molecules.

ACKNOWLEDGEMENT

A. Malek and M. Eikerling gratefully acknowledge financial support toward this project from the NSERC APC network CaRPE-FC. The DFT calculations were performed by support provided by WestGrid (www.westgrid.ca) and Compute Canada (www.computecanada.ca).

REFERENCES

1. H. A. Gasteiger, S. S. Kocha, B. Sompalli, F. T. Wagner, Appl. Catal. B Environ. **56**, 9–35 (2005).
2. M. Eikerling, A. Kulikovsky, Polymer Electrolyte Fuel Cells: Physical Principles of Materials and Operation. (CRC Press, Boca Raton, 2014).
3. M. J. Eslamibidgoli, J. Huang, T. Kadyk, A. Malek, M. Eikerling, Nano Energy **29**, 334–361 (2016).
4. O. T. Holton, J. W. Stevenson, Platin. Met. Rev. **57**, 259–271 (2013)
5. M. K. Debe, Nature **486**, 43–51 (2012).
6. M. Busch, N. B. Halck, U. I. Kramm, S. Siahrostami, P. Krtil, J. Rossmeisl, Nano Energy **29**, 126–135 (2016).
7. J. K. Norskov, J. Rossmeisl, A. Logadottir, L. Lindqvist, J. R. Kitchin, T. Bligaard, H. Jonsson, J. Phys. Chem. B **108**, 17886–17892 (2004).
8. V. Stamenkovic, B. S. Mun, K. J. J. Mayrhofer, P. N. Ross, N. M. Markovic, J. Rossmeisl, J. Greeley, J. K. Norskov, Angew. Chem. Int. Ed. **45**, 2897–2901 (2006).
9. V. Tripkovic, E. Skulason, S. Siahrostami, J. K. Norskov, J. Rossmeisl, Electrochim. Acta **55**, 7975–7981 (2010).
10. U.S. Department of Energy Hydrogen and Fuel Cells Program, "Record 15015: Fue Cell System Cost – 2015, doi:http://www.hydrogen.energy.gov/program_records.html, (2015).
11. N. Guerrero Moreno, M. Cisneros Molina, D. Gervasio, J. F. Pérez Robles, Renew. Sust. Energ. Rev. **52**, 897–906 (2015).
12. M. Lee, M. Uchida, H. Yano, D. A. Tryk, H. Uchida, M. Watanabe, Electrochim. Acta **55**, 8504–8512 (2010).
13. E. Sadeghi, A. Putz, M. Eikerling, J. Electrochem. Soc. **160**, F1159–F1169 (2013).
14. R. Borup, J. Meyers, B. Pivovar, Y. S. Kim, R. Mukundan, N. Garland, D. Myers, M. Wilson, F. Garzon, D. Wood, P. Zelenay, K. More, K. Stroh, T. Zawodzinski, J. Boncella, J. E. McGrath, M. Inaba, K. Miyatake, M. Hori, K. Ota, Z. Ogumi, S. Miyata, A. Nishikata, Z. Siroma, Y. Uchimoto, K. Yasuda, K. I. Kimijima, N. Iwashita, Chem. Rev. **107**, 3904–3951 (2007).
15. K. Yu, D. J. Groom, X. P. Wang, Z. W. Yang, M. Gummalla, S. C. Ball, D. J. Myers, P. J. Ferreira, Chem. Mater. **26**, 5540–5548 (2014).
16. S. G. Rinaldo,W. Lee, J. Stumper,M. Eikerling, Electrocatalysis, **5**, 262–272 (2014).
17. P. Urchaga, T. Kadyk, S. G. Rinaldo, A. O. Pistono, J. Hu, W. Lee, C. Richards, M. H. Eikerling, C. A. Rice, Electrochim. Acta **176**, 1500–1510 (2015).

18. I. E. L. Stephens, A. S. Bondarenko, F. J. Perez-Alonso, F. Calle-Vallejo, L. Bech, T. P. Johansson, A. K. Jepsen, R. Frydendal, B. P. Knudsen, J. Rossmeisl, I. Chorkendorff, J. Am. Chem. Soc. **133**, 5485–5491 (2011).
19. I. E. L. Stephens, A. S. Bondarenko, U. Gronbjerg, J. Rossmeisl, I. Chorkendorff, Energ. Environ. Sci. **5**, 6744–6762 (2012).
20. L. Y. Wang, A. Roudgar, M. Eikerling, J. Phys. Chem. C **113**, 17989–17996 (2009).
21. V. R. Stamenkovic, B. S.Mun, M. Arenz, K. J. J.Mayrhofer, C. A. Lucas, G. F.Wang, P. N. Ross, N.M. Markovic, Nat. Mater. **6**, 241–247 (2007).
22. A. A. Topalov, S. Cherevko, A. R. Zeradjanin, J. C. Meier, I. Katsounaros, K. J. J. Mayrhofer, Chem. Sci. **5**, 631–638 (2014).
23. I. Katsounaros, S. Cherevko, A. R. Zeradjanin, K. J. J. Mayrhofer, Angew. Chem. Int. Ed. 53, 102–121 (2014) 24. R. M. Darling, J. P. Meyers, J. Electrochem. Soc. **150**, A1523– A1527 (2003).
25. S. G. Rinaldo, J. Stumper, M. Eikerling, J. Phys. Chem. C **114**, 5773–5785 (2010)
26. J. Rossmeisl, K. Chan, E. Skúlason,M. E. Björketun, V. Tripkovic, Catal. Today **262**, 36–40 (2016).
27. V. A. T. Dam, F. A. de Bruijn, J. Electrochem. Soc. **154**, B494– B499 (2007)
28. G. Jerkiewicz, G. Vatankhah, J. Lessard, M. P. Soriaga, Y. S. Park, Electrochim. Acta **49**, 1451–1459 (2004).
29. Y. Furuya, T. Mashio, A. Ohma, N. Dale, K. Oshihara, G. Jerkiewicz, J. Chem. Phys. **141**, 164705 (2014).
30. J. Huang, A. Malek, J. Zhang, M. H. Eikerling, J. Phys. Chem. C **120**, 13587–13595 (2016).
31. U. Benedikt, W. B. Schneider, A. A. Auer, Phys. Chem. Chem. Phys. **15**, 2712–2724 (2013).
32. C. D. Taylor, M. Neurock, Curr. Opin. Solid StateMater. Sci. **9**, 49–65 (2005)
33. J. Rossmeisl, K. Chan, R. Ahmed, V. Tripkovic, M. E. Bjorketun, Phys. Chem. Chem. Phys. **15**, 10321–10325 (2013).
34. M. E. Bjorketun, J. Rossmeisl, K. R. Chan, Z. H. Zeng, R. Ahmed, V. Tripkovic, Abstr. Pap. Am. Chem. Soc. **246** (2013).
35. J. Rossmeisl, J. K. Norskov, C. D. Taylor, M. J. Janik, M. Neurock, J. Phys. Chem. B **110**, 21833–21839 (2006).
36. C. D. Taylor, S. A. Wasileski, J. S. Filhol, M. Neurock, Phys. Rev. B **73**(16), (2006).
37. N. Bonnet, N. Marzari, Phys. Rev. Lett. **110**, 086104 (2013).
38. S. Iyemperumal, N. A. Deskins, ChemPhysChem **18**, (2017).
39. C.M. Gray, K. Saravanan, G.Wang, J. A. Keith, Mol. Simul. **43**(5–6), 420–427 (2017).
40. Y. Gohda, S. Schnur, A. Gross, Faraday Discuss. **140**, 233–244 (2008).

41. S. Schnur, A. Groß, New J. Phys. **11**, 125003 (2009).
42. A. Gross, F. Gossenberger, X. H. Lin, M. Naderian, S. Sakong, T. Roman, J. Electrochem. Soc. **161**, E3015–E3020 (2014).
43. S. Sakong, M. Naderian, K. Mathew, R. G. Hennig, A. Gross, J. Chem. Phys. **142**, 234107 (2015).
44. V. Tripkovic, M. E. Björketun, E. Skúlason, J. Rossmeisl, Phys. Rev. B **84**, 115452 (2011).
45. M. A. Henderson, Surf. Sci. Rep. **46**, 1–308 (2002).
46. P. A. Thiel, T. E. Madey, Surf. Sci. Rep. **7**, 211–385 (1987).
47. H. Ogasawara, B. Brena, D. Nordlund, M. Nyberg, A. Pelmenschikov, L. G. Pettersson, A. Nilsson, Phys. Rev. Lett. **89**, 276102 (2002).
48. T. Schiros, L. A. Naslund, K. Andersson, J. Gyllenpalm, G. S. Karlberg, M. Odelius, H. Ogasawara, L. G. M. Pettersson, A. Nilsson, J. Phys. Chem. C **111**, 15003–15012 (2007).
49. A. Hodgson, S. Haq, Surf. Sci. Rep. **64**, 381–451 (2009).
50. S. Schnur, A. Gross, New J. Phys. **11**, 125003 (2009).
51. J. Carrasco, A. Hodgson, A. Michaelides, Nat. Mater. **11**, 667–674 (2012).
52. G. Kresse, J. Hafner, Phys. Rev. B Condens. Matter **47**, 558–561 (1993).
53. G. Kresse, J. Hafner, Phys. Rev. B Condens. Matter **49**, 14251–14269 (1994).
54. G. Kresse, J. Furthmüller, Comput. Mater. Sci. **6**, 15–50 (1996).
55. G. Kresse, J. Furthmuller, Phys. Rev. B Condens. Matter **54**, 11169–11186 (1996).
56. Y. K. Zhang, W. T. Yang, Phys. Rev. Lett. **80**, 890–890 (1998).
57. J. P. Perdew, K. Burke, M. Ernzerhof, Phys. Rev. Lett. **77**, 3865– 3868 (1996).
58. P. E. Blochl, Phys. Rev. B **50**, 17953–17979 (1994).
59. P. Vassilev, R. A. van Santen, M. T. M. Koper, J. Chem. Phys. **122**, 054701 (2005).
60. J. G. Wang, B. Hammer, J. Chem. Phys. **126**, 184704 (2007).
61. L. Bengtsson, Phys. Rev. B **59**, 12301–12304 (1999).
62. R. B. Getman, Y. Xu,WF. Schneider, J. Phys. Chem. C **112**, 9559– 9572 (2008).
63. M. Wakisaka, Y. Udagawa, H. Suzuki, H. Uchida, M. Watanabe, Energy Environ. Sci. **4**, 1662–1666 (2011).
64. S. K. Jo, J. White, Surf. Sci. **261**, 111–117 (1992).
65. G. B. Fisher, Chem. Phys. Lett. **79**, 452–458 (1981).
66. G. N. Derry, J. Z. Zhang, Phys. Rev. B **39**, 1940–1941 (1989).
67. F. Gossenberger, T. Roman, K. Forster-Tonigold, A. Gross, Beilstein J. Nanotechnol. **5**, 152–161 (2014).
68. D. H. Parker, M. E. Bartram, B. E. Koel, Surf. Sci. **217**, 489–510 (1989).
69. J. Neugebauer, M. Scheffler, Phys. Rev. B **46**, 16067 (1992).
70. H. Thirumalai, J. R. Kitchin, Surf. Sci. **650**, 196 (2015).
71. N. E. Singh-Miller, N. Marzari, Phys. Rev. B **80**(23), 235407 (2009).

72. A. Patra, J. Bates, J. Sun, J. P. Perdew, arXiv preprint arXiv: 1702.08515, (2017).
73. C. Fall, N. Binggeli, A. Baldereschi, J. Phys. Condens. Matter **11**(13), 2689 (1999).
74. S. DeWaele, K. Lejaeghere, M. Sluydts, S. Cottenier, Phys. Rev. B **94**(23), 235418 (2016).
75. S. Badwal, T. Bak, S. Jiang, J. Love, J. Nowotny, M. Rekas, C. Sorrell, E. Vance, J. Phys. Chem. Solids **62**(4), 723–729 (2001).
76. M. Kaack, D. Fick, Surf. Sci. **342**(1–3), 111–118 (1995).
77. M.P. Hyman, J.W. Medlin, J. Phys. Chem. B **109**(13), 6304–6310 (2005).
78. T. C. Leung, C. L. Kao, W. S. Su, Y. J. Feng, C. T. Chan, Phys. Rev. B **68**(19), 195408–195404 (2003).
79. A.J. Bard, L.R. Faulkner, Fundamentals and Applications. Electrochemical Methods, 2nd edn. (Wiley, New York, 2001).
80. E. Langenbach, A. Spitzer, H. Lüth, Surf. Sci. **147**(1), 179–190 (1984).
81. I. Villegas, M.J. Weaver, J. Phys. Chem. **100**(50), 19502–19511 (1996).
82. S. Schnur, A. Groß, Catal. Today **165**(1), 129–137 (2011).
83. S. Grimme, J. Antony, S. Ehrlich, H. Krieg, J. Chem. Phys. **132**(15), 154104 (2010).

Tables

Table 1 Comparison of Calculated work function change for (i) symmetric slab without dipole correction and (ii) asymmetric slab with dipole correction with experimental data.

θ	$\Delta\Phi_{sym.}^{Eq.\ 3}(eV)$	$\Delta\Phi_{asym.}^{Eq.\ 3}(eV)$	$\Delta\Phi_{exp.}(eV)$
0.11	0.09	0.055	0.077
0.25	0.25	0.14	0.17
0.33	0.31	0.27	0.23
0.5	0.50	0.27	0.35
0.77	0.67	0.45	0.47
1	0.86	0.66	

Table 2 Dipole layer thickness, average fractional charges, the net partial charge number of oxide layer, $\zeta(e_0)$, and average dipole moment per Pt atom, extracted from simulations for p(2x2), p(3x3), $p(2\sqrt{3}\times 2\sqrt{3})$ R30° and p(4x4) unit cells.

θ	δ_{PtO}(Å)	$\varsigma(e_0)$	μ_{site}(D)	μ_{PtO}(D/Å^2)
***p*(2x2)**				
0.25	1.953	0.0139	-0.0326	-0.0046
0.5	1.8918	0.0106	-0.0483	-0.0069
0.75	1.8288	0.0117	-0.0772	-0.011
1	1.8179	0.0128	-0.1122	-0.016
***p*(3x3)**				
0.11	1.8651	0.02	-0.0199	-0.0028
0.33	1.9017	0.0177	-0.054	-0.0077
0.55	1.8378	0.0148	-0.0729	-0.0104
0.77	1.8251	0.0122	-0.0836	-0.0119
1	1.8202	0.0147	-0.1288	-0.0184
***p*(2√3×2√3)R30°**				
0.083	1.86	0.0184	-0.0137	-0.0019
0.25	1.9516	0.0149	-0.0349	-0.0049
0.5	1.8935	0.0124	-0.0564	-0.008
0.75	1.8263	0.0124	-0.0815	-0.0116
1	1.8178	0.0149	-0.1305	-0.0186
***p*(4x4)**				
0.0625	1.847	0.0324	-0.018	-0.0025
0.25	1.9503	0.0159	-0.0372	-0.0053
0.5	1.898	0.0112	-0.0511	-0.0073
0.75	1.8261	0.0127	-0.0841	-0.012
1	1.8177	0.0153	-0.1343	-0.0191

1

2

3

4

5

6

7